Crystal structure of a human CD3-ε/δ dimer in complex with a UCHT1 single-chain antibody fragment

Kelly L. Arnett*†, Stephen C. Harrison*†, and Don C. Wiley‡§

*Department of Biological Chemistry and Molecular Pharmacology, Howard Hughes Medical Institute, Harvard Medical School, 250 Longwood Avenue, Boston, MA 02115; and ‡Department of Molecular and Cellular Biology, Howard Hughes Medical Institute, Harvard University, Cambridge, MA 02138

The α/β T cell receptor complex transmits signals from MHC/peptide antigens through a set of constitutively associated signaling molecules, including CD3-ε/γ and CD3-ε/δ. We report the crystal structure at 1.9-Å resolution of a complex between a human CD3-ε/δ ectodomain heterodimer and a single-chain fragment of the UCHT1 antibody. CD3-ε/δ and CD3-ε/γ share a conserved interface between the Ig-fold ectodomains, with parallel packing of the two G strands. CD3-δ has a more electronegative surface and a more compact Ig fold than CD3-γ; thus, the two CD3 heterodimers have distinctly different molecular surfaces. The UCHT1 antibody binds near an acidic region of CD3-ε opposite the dimer interface, occluding this region from direct interaction with the TCR. This immunodominant epitope may be a uniquely accessible surface in the TCR/CD3 complex, because there is overlap between the binding site of the UCHT1 and OKT3 antibodies. Determination of the CD3-ε/δ structure completes the set of TCR/CD3 globular ectodomains and contributes information about exposed CD3 surfaces.

antibody-binding site | CD3 | T cell receptor

The α/β T cell receptor (TCR) is a multimeric cell-surface complex comprising a clonotypic antigen-binding TCR heterodimer and three conserved signal transducing modules: CD3-ε/γ and CD3-ε/δ heterodimers and a TCR-ζ homodimer (1–3). TCR/CD3 chains assemble into a minimal eight-subunit complex in the endoplasmic reticulum through a series of dimeric and trimeric interactions with a stoichiometry of one TCR-α/β heterodimer, one CD3-ε/γ heterodimer, one CD3-ε/δ heterodimer, and a TCR-ζ homodimer (4–8). Whereas extracellular contacts are sufficient for interactions within TCR and CD3 heterodimers (9–12), transmembrane interactions are necessary for assembly and surface expression of intact TCR/CD3 complexes (7, 13–18). Extracellular domains of CD3 may provide additional specificity to mandatory transmembrane interactions (8, 19, 20), but specific extracellular interactions between TCR and CD3-ε/δ or CD3-ε/γ have yet to be determined.

Antibodies to CD3, first used to identify and characterize T cells, are effective laboratory tools for activation of many pathways in the T cell signaling cascade. One such antibody is UCHT1 (21). Fusions of UCHT1 with immunotoxins are being used for targeted T cell depletion in animal models of organ transplantation (22). UCHT1 and several other anti-CD3 antibodies, including OKT3, recognize epitopes on CD3-ε found in heterodimers with CD3-δ and with CD3-γ, but not CD3-ε expressed in isolation (23). Understanding the specific interactions between UCHT1 and CD3 may facilitate development of this or other antibodies as clinical agents. Moreover, because UCHT1 immunoprecipitates all TCR and CD3 components, it is a good tool for studying accessible surfaces of CD3 in the TCR/CD3 complex.

Detailed structural knowledge of the TCR/CD3 complex is important for understanding how the TCR transmits the signal it receives from its MHC/peptide ligand. The structure of the TCR/CD3 complex and its relationship with other TCR/CD3 complexes and coreceptors must determine the mechanism of initial signal transduction. A conformational change in the cytoplasmic domain of CD3-ε is one of the earliest events in T cell activation (24). This change can be induced by monovalent anti-CD3 antibodies but is insufficient for T cell activation, and the cause of this change remains unclear. It has not been determined whether a conformational change within a single TCR/CD3 complex or rearrangement or oligomerization of multiple TCR/CD3 complexes induces downstream signaling events. Toward the goal of a picture of TCR/CD3/coreceptor interactions, structures of extracellular domains of human TCR-α/β, TCR-γ/δ, CD8, CD4, and CD3-ε/γ have been determined (12, 25–28). We have determined the crystal structure of a human CD3-ε/δ extracellular domain dimer complexed with a variable-domain fragment of the antibody UCHT1. This structure completes the catalog of TCR/CD3 ectodomains and constrains possible models for the complete assembly.

Materials and Methods

Design of Constructs and Bacterial Expression. Human CD3-ε and CD3-δ ectodomain constructs were each modified by PCR and inserted into a bacterial expression plasmid, pLM1 (29). The CD3-ε construct encodes residues 1–105, and the CD3-δ construct encodes residues 1–79. The UCHT1-scFv construct in the pET17b expression vector (Novagen) was provided by David Neville (National Institute of Mental Health, Bethesda) (30) and encodes residues 1–107 of the light chain at the N terminus, a 15-residue linker, and residues 1–122 of the heavy chain at the C terminus. Proteins were expressed individually in BL21(DE3) cells grown in rich medium (20 g/liter tryptone/10 g/liter yeast extract/5 g/liter NaCl/2% glycerol/50 mM K_2HPO_4/10 mM $MgCl_2$/1% glucose/100 mg/liter ampicillin), induced at log phase with 1 mM IPTG, and grown for 2–4 h. Each component formed insoluble inclusion bodies, which were purified as described (10), and solubilized in urea or guanidine-HCl. Typical yields were 100–200 mg per liter of cells.

Refolding the CD3-ε/CD3-δ/UCHT1 Complex. Refolding experiments were based on protocols described in ref. 10. In brief, 4–6 μM each of CD3-ε, CD3-δ, and UCHT1-sFv solubilized inclusion bodies were mixed, injected into cold refolding buffer (1 M L-Arg/100 mM Tris, pH 8.3/2 mM EDTA/3.6 mM cystamine/6.7 mM cysteamine), and incubated for 24–48 h. Refolding reaction mixtures were then dialyzed twice for 24 h against 10-fold excess 10 mM Tris, pH 8.0. The protein complex was concentrated on a DE52 anion exchange column and purified by size exclusion chromatography (Superdex 200, Pharmacia) and anion exchange (Mono Q, Pharmacia). Purified protein was concentrated and exchanged into 10 mM Tris, pH 8.0. This

---

procedure produced a 1:1:1 complex at low yield (2–3 mg/liter refolding mixture and 1–2% refolding efficiency). The protein preparation used in the crystals described here was dominated by disulfide-linked heterodimers. Other preparations of the complex resulted in a near equimolar mix of covalent and noncovalent dimers, which also crystallized.

Crystallization and Structure Determination. The purified CD3-ε/CD3-δ/UCHT1-scFv complex (concentrated to 10 mg/ml) crystallized in 26% PEG3350, 0.2 M NaCl, and 0.1 M Hepes, pH 7; crystals were frozen in 20% PEG8000, 30% PEG400, 0.2 M NaCl, and 0.1 M Hepes, pH 7. A data set extending to spacings of 1.9 Å was collected at the Advanced Light Source beamline 8.2.1. Data were processed by using HKL-2000 (HKL Research, Charlottesville, VA) (31). The crystal belongs to space group $P2_12_12_1$ (a = 64.87, b = 79.33, and c = 150.75) with two complexes per asymmetric unit. We determined the structure by molecular replacement, implemented with MOLREP (32), using 244 antibody fragments as search models. We used omit maps to eliminate incorrect solutions and to verify the correct one (Protein Data Bank entry 6FAB). We built an initial model with ARP/WARP (33) and completed the structure by rounds of manual rebuilding with O (34) and position, torsion angle, and B-factor refinement with CNS (35). After refinement, R_{work} = 20% and R_{free} = 24%. For data collection and refinement statistics, see Table 1, which is published as supporting information on the PNAS web site. Interatomic contacts and buried molecular surface area were calculated by using CONTACT and AREAIMOL, respectively (36). Figures were generated by using MOLSCRIPT (37) and SPOCK (38).

Results

Refolding with UCHT1-scFv Stabilizes the CD3-ε/δ Heterodimer. Preliminary attempts to refold significant amounts of CD3-ε/δ ectodomain heterodimers from *Escherichia coli*-expressed inclusion bodies were unsuccessful, in contrast to experience with CD3-ε/γ (data not shown). To stabilize the CD3-ε/δ heterodimer, human CD3-ε (residues 1–105) and CD3-δ (residues 1–79) were refolded in the presence of a single-chain variable domain fragment (scFv) of the antibody UCHT1. This procedure produced a 1:1:1 complex among CD3-ε, CD3-δ and UCHT1-scFv, with a mass consistent with a monomeric complex. The complex was stable through all steps of purification, confirming the high affinity of UCHT1 for CD3 heterodimers.

Structure Determination of the CD3-ε/δ/UCHT1-scFv Complex. Using x-ray diffraction, we determined the three-dimensional structure of the CD3-ε/CD3-δ/UCH1-scFv complex by molecular replacement to 1.9 Å (Fig. 1a). Although present in the molecule crystallized, the first 11 residues of CD3-ε had no corresponding electron density. The two complexes in the asymmetric unit differ at the C terminus; in one of the complexes, the last seven residues of CD3-ε and δ are not observed; in the other, weak electron density is observed through Cys-101 of CD3-ε and through Gln-73 of CD3-δ. Residues 54–62 (the F-G loop) of CD3-δ are disordered in both copies of the structure described here. For illustration purposes, the CD3-δ F-G loop was modeled by using weakly observed density from a second data set, but the loop is poorly ordered. The linker between the light chain and the heavy chain of the scFv fragment was disordered in all structures.

Structure of Human CD3-ε/δ. Human CD3-ε and CD3-δ are members of the Ig superfamily and adopt a similar fold (Fig. 1). Human CD3-ε has an eight-stranded I-set Ig fold (39), with two antiparallel β sheets, an ABED sheet and a C′CFG sheet. A disulfide bridge between εCys-28 and εCys-77 connects the top of the B strand to the F strand. CD3-δ has a compact seven-
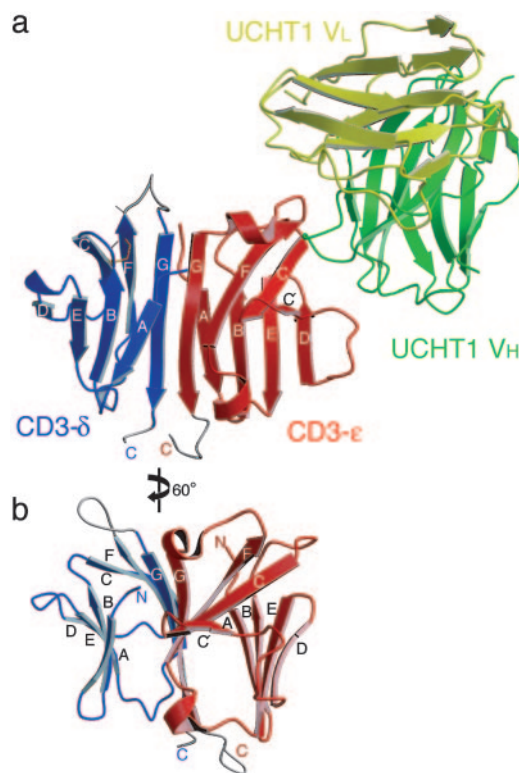
Fig. 1. Structure of the CD3-ε/δ/UCHT1-scFv complex and topology of the CD3-ε/δ dimer. (a) Ribbon diagram illustrating CD3-ε (red), CD3-δ (blue), UCHT1 heavy chain variable domain (green), and UCHT1 light chain variable domain (yellow). The eight CD3-ε strands and seven CD3-δ strands are labeled A-G by using standard nomenclature for I-set and C1-set Ig folds, respectively. Residues modeled using weak density or density from the second data set are in gray. Glycosylation sites of CD3-δ at Asn-17 and Asn-53 (gray sticks) are marked, although no glycans are present in this bacterially expressed protein. Disulfide bonds between B and F strands are in orange. (b) Sixty-degree rotation of the CD3-ε/δ dimer around the axis formed by G-strand pairing at the dimer interface.

stranded C1-set Ig fold with an ABED sheet and a CFG sheet, with a disulfide bridge between δCys-16 and δCys-52 connecting the tops of the B and F strands. The two putative N-linked glycosylation sites on CD3-δ, δAsn-17 and δAsn-53, are the first residues of the loops after the disulfide-linked Cys residues of the B and F strands. These Asn side chains point up and away from each other and from the protein core. Despite a mere 7% identity between the human CD3-ε and CD3-δ sequences, 45 core residues of the Ig domains (parts of the A, B, D, E, F, and G strands) superimpose with an rms deviation of 1.9 Å.

The ε/δ dimer interface buries a molecular surface of 1,736 Å², with extensive hydrophobic interactions, 13 hydrogen bonds, and two salt bridges. It is a noncanonical Ig interface with parallel pairing of the two G strands, creating an extended β-sheet that traverses the dimer. The CD3-ε contact surface includes four residues of the A strand (εPro-14, εTyr-15, εVal-17, and εIle-19), εAsp-42 (in C-C′ loop), εTyr-74 of the F strand, and all G strand residues (ε89–ε96). The CD3-δ contact surface includes five residues from the A strand (δLys-2, δIle-3, δPro-4, δIle-5, and δGlu-7), residues δGlu-24 and δIle-49, and all residues in the G strand (δ64–δ72). Residues of the two G strands form eight main-chain hydrogen bonds and contribute to a tyrosine ladder (εTyr-90, εTyr-74, εTyr-92, and δTyr-69) that packs against the CD3-δ A strand. Two salt bridges (δLys-2 to εAsp-42 and δGlu-7 to εArg-94) connect the CD3-δ A strand to the turn between the C and C′ strands and to the CD3-ε G

strand. As a result of the side-to-side dimer interface, CD3 is flat and elongated, with faces more than twice as wide as the sides.

It has been proposed that the putative stem region forms part of a rigid stalk created by the G strand pairing (11). Our data indicate that this is not the case for refolded ectodomains. The CD3 complex described here contains the complete ectodomains of both CD3-ε and CD3-δ, but weak or no density was observed for the CxxC motif. See *Supporting Text*, which is published as supporting information on the PNAS web site, for further discussion of this issue.

Comparison with CD3-ε/γ: Conserved Dimer Interface and Divergent Molecular Surfaces. The overall fold, and particularly the dimer interface, is conserved among the structures of human CD3-ε/δ described here, mouse CD3-ε/γ previously determined by NMR spectroscopy (11), and human CD3-ε/γ recently determined by x-ray crystallography (12) (Fig. 2a). Human CD3-ε adopts a nearly identical fold in complexes with CD3-γ and CD3-δ, with an rms deviation of 1.1 Å for 83 superimposed Cα atoms, with only minor deviations in loop regions. In human and mouse CD3-ε, 61 Cα atoms superimpose with an rms deviation of 1.3 Å. Among known CD3-ε proteins, human CD3-ε has a unique insertion after the C′ strand created by an apparent duplication event. This insertion forms an acidic loop and the D strand. CD3-δ and CD3-γ, which share more sequence identity with each other than with CD3-ε, have seven-stranded Ig folds, and, in human CD3-δ and CD3-γ, 50 Cα atoms superimpose with an rms deviation of 1.5 Å. Human CD3-δ has a C1-set Ig fold with a short D strand; both mouse and human CD3-γ have C2-set Ig folds with a short C′ strand (11, 12). The G strands of CD3-δ and CD3-γ, which share a QVxYRMC motif, superimpose at the dimer interfaces of hCD3-ε/γ and hCD3-ε/δ, conserving the main-chain hydrogen bonds and aromatic ladder (Fig. 2b). CD3-δ and CD3-γ also share an LGxxxxDPR motif, which forms part of the E strand and the proline-mediated turn connecting a short helix to the F strand.

In addition to shared conserved residues, CD3-γ and CD3-δ have features unique to the subtype but conserved across species. CD3-δ has a shorter B-C loop and a longer and more flexible F-G loop than CD3-γ. Unlike CD3-γ and CD3-ε, CD3-δ has only two residues N-terminal to the A strand. The C strand and the tops of the F and G strands of CD3-δ are shifted in toward the dimer interface and remain almost parallel to the G strand of CD3-ε. In the CD3-ε/γ structures, this sheet bends away more from the dimer interface. Because of these differences, CD3-δ has a more compact Ig fold than CD3-γ.

CD3-ε/γ and CD3-ε/δ dimers have strikingly different surface electrostatic potentials (Fig. 2c). CD3-γ has an electropositive surface and a pI of 9 for the extracellular domain; CD3-δ is more electronegative, with a pI of 5. Both faces of CD3-δ and the side are significantly more electronegative than the equivalent surfaces of CD3-γ. Unlike CD3-ε, for which most of the conserved residues are buried within the Ig fold or at the heterodimer interface, CD3-δ has 13 conserved, surface-exposed residues, 11 of which are not found in CD3-γ (Fig. 3). A notable patch of highly conserved, mostly charged surface residues (δGlu-9, δAsp-10, δArg-11, δLys-41, and δIle-43) forms the A-B and E-F loops and covers the base of the CD3-δ side of the dimer (Fig. 3b). These conserved surface residues unique to CD3-δ may be a potential binding site for TCR or possibly for coreceptor CD4 or CD8.

The UCHT1 Antibody Fragment Binds Near a Large Acidic Surface on CD3-ε. UCHT1-scFv, which interacts with both CD3-ε/γ and CD3-ε/δ heterodimers, binds a large nonlinear surface epitope, which includes part of an extensive acidic surface of CD3-ε opposite the heterodimer interface (Fig. 4). The UCHT1-scFv:CD3-ε/δ interface has a buried molecular surface of 1,789
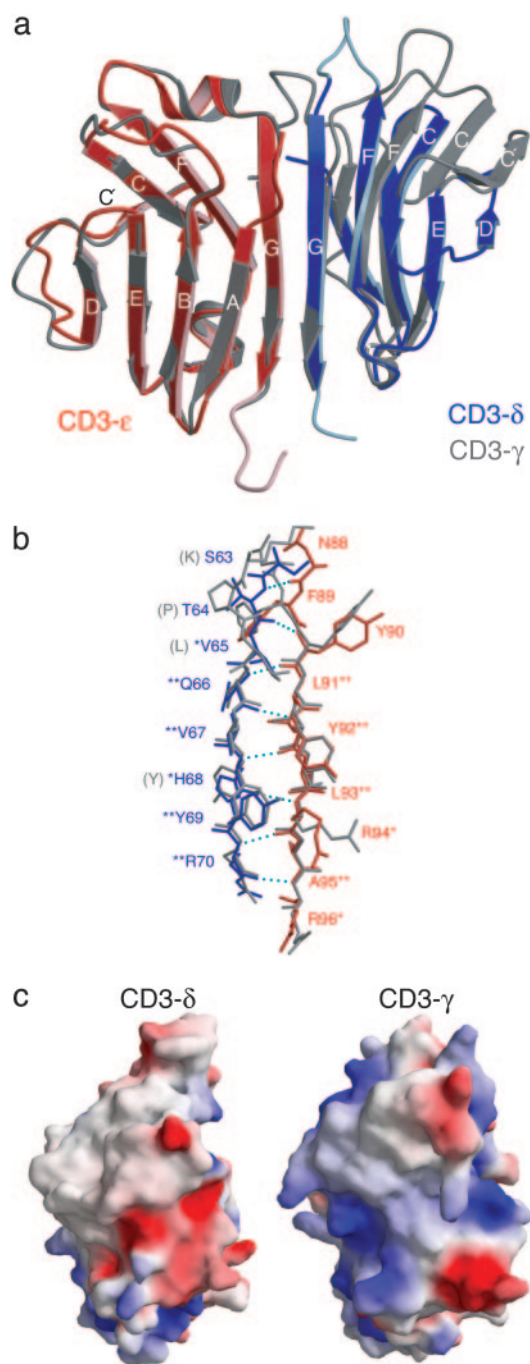
Fig. 2. Comparison of human CD3-ε/δ and human CD3-ε/γ. (a) Overlay of CD3-ε/δ (red/blue) and CD3-ε/γ (gray), created by superimposing the CD3-ε subunits. (b) Backbone and side-chain detail of G-strand pairing of CD3 dimers. Main-chain hydrogen bonds between CD3-ε and CD3-δ are shown as dotted cyan lines. Residues absolutely conserved between CD3-γ and CD3-δ or residues conserved among mammalian CD3-ε are labeled with **; those that conserve similarity are labeled with *. Human CD3-γ residue differences are indicated in parentheses. (c) Positive and negative electrostatic surface potentials (blue and red, respectively) of CD3-ε/δ and CD3-ε/γ dimers. The view is a 90° rotation from the one in a, showing a side view of CD3-δ and CD3-γ on the left and right, respectively. In contrast to CD3-γ, which has an electropositive surface, both CD3-ε and CD3-δ are electronegative.

Å², above the average of 1,680 Å² for known antibody/protein antigen interfaces (40). UCHT1 contacts 15 CD3-ε residues in the B-C, C′-D, and F-G loops and in the C′, D, and F strands.
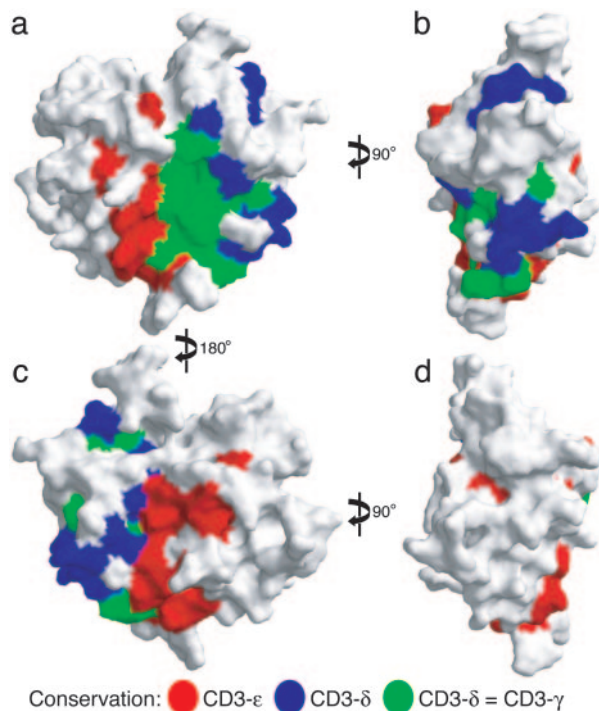
Fig. 3. Molecular surface representations of CD3-ε/δ conservation. Residues conserved among mammalian CD3-ε molecules (red), residues conserved between CD3-δ and CD3-γ (green), and residues conserved among CD3-δ molecules but not found in CD3-γ (blue) are colored. (*a*) ''Front'' face of CD3-ε/δ oriented such that the C-terminal residues of CD3-ε and CD3-δ are at the bottom and CD3-ε and CD3-δ subunits are side-to-side, as in Fig. 2*a*. (*b*) Side of CD3-δ. (*c*) ''Back'' face of CD3-ε/δ, as in Fig. 1 (a 180° rotation of *a*). (*d*) Side of CD3-ε. The front, back, and CD3-δ side of the dimer have clusters of conserved surface residues. The CD3-ε side of the dimer is devoid of conserved regions.

The contacts include two salt bridges, six side-chain-to-side-chain hydrogen bonds, and five side-chain-to-main-chain hydrogen bonds, as well as van der Waals contacts, which are predominantly mediated by six aromatic residues on UCHT1. Heavy-chain hypervariable residues insert into the groove created by the F-G loop and the C′ strand, and light-chain residues contact the opposite side and top of this ridge formed by the protruding F-G loop. Comparison with the structure of human CD3-ε/γ bound by the OKT3 Fab (12) reveals an overlap in the binding sites for these two antibodies. OKT3 buries only 1,220 Å^2 and contacts residues ε35, ε47, ε49, and ε80–86 (12). UCHT1 contacts all of these residues, as well as residues ε44, ε45, ε48, ε56, and ε78. The binding site extends more deeply into the groove between the F-G loop and C′ strand and further down the side of CD3-ε.

Discussion

In their role as TCR-associated signal transducing dimers, CD3-ε/δ, CD3-ε/γ and TCR-ζ transmit intercellular signals initiated through TCR:MHC/peptide-ligand engagement, resulting in recruitment of Nck, activation of tyrosine kinase activity, phosphorylation of the cytoplasmic immunoreceptor tyrosine-based activation motifs, and other downstream signaling events (41). Our crystal structure of human CD3-ε/δ in complex with a single-chain variable domain fragment of the antibody UCHT1 contributes the last unknown extracellular component of the TCR/CD3 complex and enables us to discuss models for the entire assembly of ectodomains. CD3-ε/δ, like CD3-ε/γ, has a continuous β-sheet, which traverses the dimer and probably imparts considerable rigidity. Therefore, we can
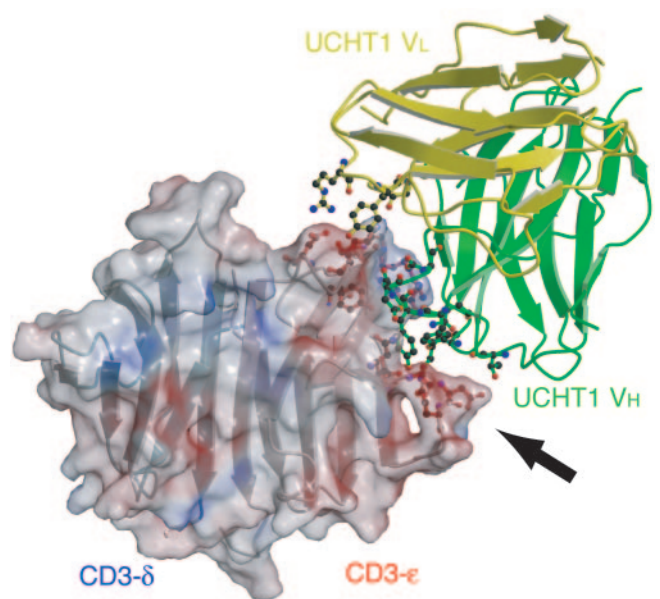
Fig. 4. Molecular surface of CD3-ε/δ and UCHT1 contact residues. Positive and negative electrostatic surface potentials of CD3-ε/δ dimer are indicated on the translucent molecular surface in blue and red, respectively. CD3-ε/δ is oriented as in Fig. 1. CD3-ε and UCHT1 contact residues, which form hydrogen bonds or salt bridges, are indicated as ball-and-stick models. UCHT1 light chain (yellow) and heavy chain (green) bind exclusively to CD3-ε near an electronegative region on the side (indicated with an arrow), partially occluding it and burying a molecular surface of 1,789 Å^2.

consider first how these two paddle-shaped structures pack against the familiar α/β-TCR heterodimer and then how the complex orients with respect to the membrane. Because our structure also identifies the binding site for the UCHT1 antibody, as well as conserved surface regions unique to CD3-ε/δ, it offers some additional information about exposed and buried surfaces.

CD3-δ and CD3-γ are derived from a common precursor by an apparent gene duplication event. They are distinct molecules only in mammals; chickens and amphibians have a single CD3-γ/δ protein (see Fig. 6, which is published as supporting information on the PNAS web site). The transmembrane and cytoplasmic domains of CD3-δ and CD3-γ are similar, but the extracellular domains have diverged substantially. CD3-ε/δ and CD3-ε/γ thus present distinct molecular and electrostatic surfaces (Figs. 2*c* and 3). Indeed, ectodomain residues conserved between CD3-δ and CD3-γ are almost exclusively at positions buried in the Ig fold or at the dimer interface with CD3-ε. We have looked for clusters of surface residues, conserved among mammals, for evidence of important contacts. CD3-ε/δ has conserved patches on the two faces and on the CD3-δ side (Fig. 3 *a–c*), each of which is near the ''bottom'' of the CD3 dimer. Some of these conserved residues are at the dimer interface, but several are solvent-exposed and unique to CD3-δ. We propose that the surfaces with conserved differences between CD3-δ and CD3-γ participate in specific interactions with the TCR (and possibly with coreceptors CD4 and CD8), and we describe below a model deriving from this proposal.

Is there a defined organization for the three heterodimeric ectodomains in the TCR/CD3 complex? Evidence has accumulated for a minimal TCR/CD3 complex containing exactly one TCR-α/β, one TCR-ζ, one CD3-ε/γ, and one CD3-ε/δ, all of which are required for its structural and functional integrity (7, 8). Trimeric transmembrane interactions, among CD3-ε, CD3-γ, and TCR-β and among CD3-ε, CD3-δ, and TCR-α, have an

IMMUNOLOGY

essential role in assembly and surface expression of TCR/CD3 complexes (7, 18), but extracellular contacts appear to enhance these interactions. For example, ectodomain interactions between TCR-β and both CD3-ε and γ protect against degradation (42), and ectodomain chimeric mutations prevent TCR-α from associating with CD3-ε/δ (43, 44). Mouse and human CD3-ε associate into the same TCR/CD3 complex (45), and TCR-α/β constant-domain chimeras from various mammalian species associate on the cell surface with human CD3 molecules, but chicken TCR-α and TCR-β do not (44). These data indicate that there are extracellular interactions between TCR and CD3 dimers involving residues conserved among mammals. Moreover, if extracellular interactions are required for specificity, then CD3-γ and CD3-δ, not just CD3-ε, must contact the TCR.

Additional information about exposed and buried surfaces derives from antibody reactivity. The UCHT1 antibody binds a nonconserved conformational epitope on the top and side of CD3-ε, opposite the dimer interface, and the UCHT1-scFv forms a stable complex with both CD3-ε/δ and CD3-ε/γ dimers (data not shown). UCHT1 immunoprecipitates intact TCR/CD3 complexes (46), so its epitope must be exposed on at least one of the cell-surface CD3-ε subunits. Because TCR/CD3-ε/δ and TCR/CD3-ε/γ hemicomplexes can also be immunoprecipitated with UCHT1 (Kai Wucherpfennig, personal communication), the epitope is probably exposed on both CD3-ε chains in a complete CD3/TCR assembly. Overlap of the binding sites for UCHT1 and a number of other antibodies to extracellular CD3, including OKT3, also suggests that this nonconserved area is exposed on cell-surface CD3. Indeed, it is probably an immunodominant epitope precisely because it is the only readily accessible part of CD3 (23). In contrast, the only antibody known to recognize the ectodomain of CD3-δ binds CD3-δ in isolation but does not bind to TCR/CD3 complexes (47). A reasonable explanation is that CD3-δ has little or no exposed immunogenic surface because it is buried in the TCR/CD3 complex by protein contacts and by glycosylation. The interaction with UCHT1 partially occludes an acidic surface on the side the CD3-ε. It has been proposed that the equivalent acidic region in mouse binds to a surface cavity of the TCR beneath the F-G loop of TCR-β constant domain (11, 48), but our structure and the immmunoprecipitation experiments make this proposal unlikely.

The conserved stems of the two CD3 heterodimers could be flexible hinges or rigid stalks connecting the extracellular domains and the transmembrane segments. To the extent that they do adopt a fixed structure, they will probably do so only in the context of a complete CD3/TCR complex, because the stems are mostly disordered in our CD3-ε/δ structure and absent from the available CD3-ε/γ structures (11, 12). The stem regions appear to have a role in heterodimerization at the cell surface (16, 18), but interchain disulfide bonds have not been detected (8). Intrachain disulfides within the CxxC, which are plausible in the oxidizing endoplasmic reticulum and extracellular environment, would shorten the span of the stems and possibly introduce kinks. We are thus led to consider models in which the paddle-shaped, CD3-ε/γ and ε/δ ectodomains lie close to the membrane, potentially with their pseudo twofold axes making sharp angles with the membrane surface rather than orienting perpendicular to it. The narrow sides of the CD3 heterodimers could permit a bend in the stem region to direct one of the faces of CD3 to lie nearly parallel to the membrane.

The TCR subunits also have stem-like regions, not included in the crystallographically determined TCR structures. These "connecting peptides," which begin at the interchain disulfide bond and include at least 21 TCR-α and 12–16 TCR-β residues, could accommodate considerable flexibility in the orientation of the TCR with respect to signaling molecules in the complex. If extended, the TCR-β connecting peptide could lift the TCR well above the membrane (30–45 Å). The TCR-α connecting peptide
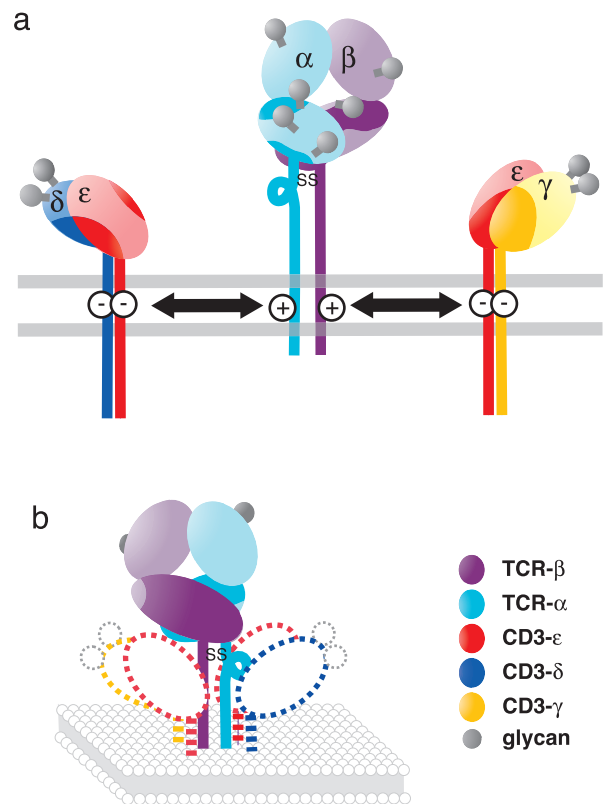
Fig. 5. Conservation of TCR/CD3 extracellular domains and proposed model for TCR/CD3 complex. (a) Schematic representation of TCR and CD3 assembly. Conserved regions are shown as bold patches. Nonconserved regions and TCR variable domains are pale. Carbohydrate moieties are gray spheres. (b) A proposed model for the TCR/CD3 complex. Its principle features are (i) the complex is tight, because trimeric transmembrane contacts among TCR/CD3 components (α-ε-δ, β-ε-γ, and α-ζ-ζ) suggest a compact bundle, perhaps no wider than the TCR alone; (ii) to create these interactions, the CD3 dimer ectodomains lie angled to the membrane between it and the TCR globular domains; and (iii) CD3-ε/γ and CD3-ε/δ interact by their heterodimeric faces with asymmetric nonglycosylated TCR surfaces that are conserved among mammals. The lengths of TCR-β and TCR-α connecting peptides missing from known structures suggest that the TCR sits "above" the CD3 dimers. The requirement that TCR and CD3 TM domains interact, the shape of the membrane-proximal surface of the TCR, and the positions of conserved residues in the three heterodimers suggest that the paddle-shaped CD3 ectodomains lie at an angle relative to the membrane. The stoichiometry and interspecies promiscuity of TCR/CD3 interactions suggest that both CD3 dimers interact through their heterodimeric faces with the conserved nonglycosylated bottom and side of the TCR. This interaction mode would allow contacts to extend to the small patches of conserved residues on the sides of CD3-γ or CD3-δ. Glycosylation of these sides in some species precludes direct side-on binding with the TCR.

has been implicated in association with CD3-ε/δ dimers (43) and with TCR-ζ (49). Because much of CD3-ε/γ and ε/δ are antigenically inaccessible, we suggest that the CD3 ectodomains may be positioned between the globular domain of the TCR and the outer membrane surface (Fig. 5). The TCR-α/β dimer has two wider sides: one, dominated by TCR-β, is conserved among mammals and not heavily glycosylated; the other, dominated by TCR-α, is variable and highly glycosylated. The former is a better candidate for interaction with CD3. Conserved surfaces on TCR-α are confined largely to the "bottom" of the molecule and to structurally undetermined regions.

The scheme in Fig. 5 summarizes these observations on regions of TCR/CD3 conservation, inter-species promiscuity, exposed and nonexposed antibody binding surfaces, sites of

glycosylation, and length and potential flexibility of nonglobular extracellular regions. In this picture, which is simply intended to illustrate what we believe will be key properties of the assembly, the two CD3 dimers bind along their faces in an asymmetric manner to unique nonglycosylated TCR surfaces on the conserved side and bottom of the TCR. The CD3 dimer faces are angled to the membrane, supporting the TCR from underneath. This arrangement allows TCR-β to associate closely with CD3-ε/γ through interactions with its conserved constant and transmembrane domains and explains the observation that one of the CD3-ε subunits is very near the constant domain F-G loop in mouse TCR-β (48). The arrangement further allows TCR-α to associate with both CD3-ε and CD3-δ through their transmembrane domains, through the connecting peptide region, and through a patch on the membrane-proximal surface of its globular constant domain. The bulky carbohydrate moieties of CD3-δ and CD3-γ point away from the TCR. Moreover, they cover potentially exposed protein surfaces, helping to account for the poor antigenicity of the CD3-δ (and CD3-γ) chains.

Positioning the CD3 dimers between the TCR globular domains and the membrane places all transmembrane domains near each other, consistent with known transmembrane interactions among TCR, CD3, and ζ. This interaction mode makes the TCR/CD3 complex more compact than a model in which CD3 and TCR interact in a side-on manner, and the compaction allows in turn for close packing of TCR/CD3 complexes with coreceptors or with other TCR/CD3 complexes at the immunological synapse.

1. Davis, M. M. & Bjorkman, P. J. (1988) *Nature* **334,** 395–402.
2. Clevers, H., Alarcon, B., Wileman, T. & Terhorst, C. (1988) *Annu. Rev. Immunol.* **6,** 629–662.
3. Letourneur, F. & Klausner, R. D. (1992) *Science* **255,** 79–82.
4. Koning, F., Maloy, W. L. & Coligan, J. E. (1990) *Eur. J. Immunol.* **20,** 299–305.
5. Manolios, N., Letourneur, F., Bonifacino, J. S. & Klausner, R. D. (1991) *EMBO J.* **10,** 1643–1651.
6. Punt, J. A., Roberts, J. L., Kearse, K. P. & Singer, A. (1994) *J. Exp. Med.* **180,** 587–593.
7. Call, M. E., Pyrdol, J., Wiedmann, M. & Wucherpfennig, K. W. (2002) *Cell* **111,** 967–979.
8. Call, M. E., Pyrdol, J. & Wucherpfennig, K. W. (2004) *EMBO J.* **23,** 2348–2357.
9. Borroto, A., Mallabiabarrena, A., Albar, J. P., Martinez, A. C. & Alarcon, B. (1998) *J. Biol. Chem.* **273,** 12807–12816.
10. Garboczi, D. N., Utz, U., Ghosh, P., Seth, A., Kim, J., VanTienhoven, E. A., Biddison, W. E. & Wiley, D. C. (1996) *J. Immunol.* **157,** 5403–5410.
11. Sun, Z. J., Kim, K. S., Wagner, G. & Reinherz, E. L. (2001) *Cell* **105,** 913–923.
12. Kjer-Nielsen, L., Dunstone, M. A., Kostenko, L., Ely, L. K., Beddoe, T., Mifsud, N. A., Purcell, A. W., Brooks, A. G., McCluskey, J. & Rossjohn, J. (2004) *Proc. Natl. Acad. Sci. USA* **101,** 7675–7680.
13. John, S., Banting, G. S., Goodfellow, P. N. & Owen, M. J. (1989) *Eur. J. Immunol.* **19,** 335–339.
14. Morley, B. J., Chin, K. N., Newton, M. E. & Weiss, A. (1988) *J. Exp. Med.* **168,** 1971–1978.
15. Alcover, A., Mariuzza, R. A., Ermonval, M. & Acuto, O. (1990) *J. Biol. Chem.* **265,** 4131–4135.
16. Blumberg, R. S., Alarcon, B., Sancho, J., McDermott, F. V., Lopez, P., Breitmeyer, J. & Terhorst, C. (1990) *J. Biol. Chem.* **265,** 14036–14043.
17. Cosson, P., Lankford, S. P., Bonifacino, J. S. & Klausner, R. D. (1991) *Nature* **351,** 414–416.
18. Kearse, K. P., Roberts, J. L. & Singer, A. (1995) *Immunity* **2,** 391–399.
19. Manolios, N., Kemp, O. & Li, Z. G. (1994) *Eur. J. Immunol.* **24,** 84–92.
20. Wileman, T., Kane, L. P. & Terhorst, C. (1991) *Cell Regul.* **2,** 753–765.
21. Beverley, P. C. & Callard, R. E. (1981) *Eur. J. Immunol.* **11,** 329–334.
22. Weetall, M., Digan, M. E., Hugo, R., Mathew, S., Hopf, C., Tart-Risher, N., Zhang, J., Shi, V., Fu, F., Hammond-McKibben, D., *et al.* (2002) *Transplantation* **73,** 1658–1666.
23. Salmeron, A., Sanchez-Madrid, F., Ursa, M. A., Fresno, M. & Alarcon, B. (1991) *J. Immunol.* **147,** 3047–3052.
24. Gil, D., Schamel, W. W., Montoya, M., Sanchez-Madrid, F. & Alarcon, B. (2002) *Cell* **109,** 901–912.
25. Garboczi, D. N., Ghosh, P., Utz, U., Fan, Q. R., Biddison, W. E. & Wiley, D. C. (1996) *Nature* **384,** 134–141.
26. Allison, T. J., Winter, C. C., Fournie, J. J., Bonneville, M. & Garboczi, D. N. (2001) *Nature* **411,** 820–824.
27. Wu, H., Kwong, P. D. & Hendrickson, W. A. (1997) *Nature* **387,** 527–530.
28. Gao, G. F., Tormo, J., Gerth, U. C., Wyer, J. R., McMichael, A. J., Stuart, D. I., Bell, J. I., Jones, E. Y. & Jakobsen, B. K. (1997) *Nature* **387,** 630–634.
29. Sodeoka, M., Larson, C. J., Chen, L., Leclair, K. P. & Verdine, G. L. (1993) *Bioorg. Med. Chem. Lett.* **3,** 1089–1094.
30. Thompson, J., Stavrou, S., Weetall, M., Hexham, J. M., Digan, M. E., Wang, Z., Woo, J. H., Yu, Y., Mathias, A., Liu, Y. Y., *et al.* (2001) *Protein Eng.* **14,** 1035–1041.
31. Otwinowski, Z. & Minor, W. (1997) in *Methods in Enzymology*, eds. Carter, C. W., Jr., & Sweet, R. M. (Academic, New York), Vol. 276, pp. 307–326.
32. Vagin, A. & Teplyyakov, A. (1997) *J. Appl. Crystallogr.* **30,** 1022–1025.
33. Perrakis, A., Morris, R. & Lamzin, V. S. (1999) *Nat. Struct. Biol.* **6,** 458–463.
34. Jones, T. A., Zou, J. Y., Cowan, S. W. & Kjeldgaard. (1991) *Acta. Crystallogr. A.* **47,** 110–119.
35. Brunger, A. T., Adams, P. D., Clore, G. M., DeLano, W. L., Gros, P., Grosse-Kunstleve, R. W., Jiang, J. S., Kuszewski, J., Nilges, M., Pannu, N. S., *et al.* (1998) *Acta. Crystallogr. D. Biol. Crystallogr.* **54,** 905–921.
36. Collaborative Computational Project, Number 4. (1994) *Acta Crystallogr. D.* **50,** 760–763.
37. Kraulis, P. J. (1991) *J. Appl. Crystallogr.* **24,** 946–950.
38. Christopher, J. A., Swanson, R. & Baldwin, T. O. (1996) *Comput. Chem.* **20,** 339–345.
39. Harpaz, Y. & Chothia, C. (1994) *J. Mol. Biol.* **238,** 528–539.
40. Lo Conte, L., Chothia, C. & Janin, J. (1999) *J. Mol. Biol.* **285,** 2177–2198.
41. Alarcon, B., Gil, D., Delgado, P. & Schamel, W. W. (2003) *Immunol. Rev.* **191,** 38–46.
42. Wileman, T., Kane, L. P., Young, J., Carson, G. R. & Terhorst, C. (1993) *J. Cell Biol.* **122,** 67–78.
43. Backstrom, B. T., Muller, U., Hausmann, B. & Palmer, E. (1998) *Science* **281,** 835–838.
44. Gouaillard, C., Huchenq-Champagne, A., Arnaud, J., Chen Cl, C. L. & Rubin, B. (2001) *Eur. J. Immunol.* **31,** 3798–3805.
45. de la Hera, A., Muller, U., Olsson, C., Isaaz, S. & Tunnacliffe, A. (1991) *J. Exp. Med.* **173,** 7–17.
46. Friedrich, B., Cantrell, D. A. & Gullberg, M. (1989) *Eur. J. Immunol.* **19,** 17–23.
47. Rubin, B., Alibaud, L., Huchenq-Champagne, A., Arnaud, J., Toribio, M. L. & Constans, J. (2002) *Scand. J. Immunol.* **55,** 111–118.
48. Ghendler, Y., Smolyar, A., Chang, H. C. & Reinherz, E. L. (1998) *J. Exp. Med.* **187,** 1529–1536.
49. Backstrom, B. T., Hausmann, B. T. & Palmer, E. (1997) *J. Exp. Med.* **186,** 1933–1938.

IMMUNOLOGY